Human Molecular Genetics, 2014, Vol. 23, No. 11 **2791–2801**
doi:10.1093/hmg/ddt572
Advance Access published on December 13, 2013

Zn^{2+} dyshomeostasis caused by loss of ATP13A2/PARK9 leads to lysosomal dysfunction and alpha-synuclein accumulation

Taiji Tsunemi and Dimitri Krainc*

Department of Neurology, Massachusetts General Hospital, Harvard Medical School, MassGeneral Institute for Neurodegenerative Disease, Charlestown, MA 02129, USA

Received August 4, 2013; Revised October 15, 2013; Accepted November 6, 2013

Mutations in ATP13A2 (PARK9) cause Kufor-Rakeb syndrome (KRS) characterized by juvenile-onset parkinsonism, pyramidal signs and dementia. PARK9 belongs to type 5 P-type ATPase with its putative function as a cation transporter. Loss of PARK9 leads to lysosomal dysfunction and subsequent α-synuclein (α-Syn) accumulation. However, the mechanistic link between PARK9 and lysosomal dysfunction remains unclear. Here, we found that patient fibroblasts expressing mutant PARK9 or primary neurons with silenced PARK9 exhibited increased sensitivity to extracellular zinc (Zn^{2+}). This effect was rescued with the Zn^{2+} chelators clioquinol or TPEN. PARK9-deficient cells showed decreased lysosomal sequestration of Zn^{2+} and increased expression of zinc transporters. Importantly, increased concentrations of Zn^{2+} (Zn^{2+} stress) resulted in lysosomal dysfunction that was partially restored by expression of wild-type PARK9. Zn^{2+} stress also caused increased expression of α-Syn and consequently decreased activity of the lysosomal enzyme glucocerebrosidase. Together, these data suggest that PARK9 loss of function leads to dyshomeostasis of intracellular Zn^{2+} that in turn contributes to lysosomal dysfunction and accumulation of α-Syn. It will be of interest to examine whether therapeutic lowering of zinc may prove beneficial for patients with KRS.

INTRODUCTION

Kufor-Rakeb syndrome (KRS) is a rare hereditary disorder that presents with parkinsonism and other neurological manifestations such as dementia and pyramidal signs (1). In 2006, analysis of a Chilean family uncovered the disease-causing mutations in *ATP13A2* which codes for P-type ATPase (ATP13A2/PARK9) (2). The frameshift mutation (c.1632_1653dup22) identified in the original family suggested that KRS was caused by a functional loss of PARK9. A number of subsequent studies have revealed that many other homozygous and compound heterozygous missense mutations in *PARK9* are linked to juvenile-onset or early-onset forms of familial or sporadic parkinsonisms (3,4). While homozygous mutations cause juvenile-onset parkinsonism, heterozygotes present with parkinsonism in midlife, indicating a gene dose effect of PARK9 (4).

PARK9 is an 1180 amino acid protein with 10 predicted transmembrane domains, expressed ubiquitously with strongest expression in CNS. High expression of PARK9 was detected in dopaminergic neurons of substantia nigra (SN) (2), and its levels were increased in the brains of sporadic Parkinson's disease (PD) patients, underscoring the involvement of PARK9 in PD pathogenesis (2,3,5).

PARK9 belongs to P-type ATPase superfamily (type 5) that is suggested to transport charged substrates across the membrane (6). Although the type 5 has no known specific substrates, based on the amino acid sequence, it has been speculated that PARK9 serves as a cation transporter. A prior study using yeast ortholog of *ATP13A2,* (Ypk9), demonstrated that PARK9-depleted *ypk9*Δ yeast cells conferred sensitivity to manganese (Mn^{2+}), whereas over-expression of wild-type Ypk9 partially reversed Mn^{2+} sensitivity (7). Another study showed that over-expression of wild-type PARK9 in HEK cells and primary rat neurons rendered cells more resistant to Mn^{2+} toxicity (8), further indicating a protective role of PARK9 against elevated levels of Mn^{2+}.

Previous work showed that exogenously expressed wild-type PARK9 localized to acidic vesicles (2,5,8). It is presumed that misfolding of mutated PARK9 in endoplasmic reticulum results

*To whom correspondence should be addressed at: MassGeneral Institute for Neurodegenerative Disease, 114 16th Street, Room 2008, Charlestown, MA02129, USA. Fax: +617 724 1480; Email: krainc@helix.mgh.harvard.edu

in its degradation by the ubiquitin proteasome pathway and deficient trafficking to the lysosome (2,5,8). We have previously documented lysosomal dysfunction in the presence of deficient PARK9 (9), suggesting its role in the normal function of lysosomes. We also found that depletion of PARK9 resulted in accumulation of α-Syn, further implicating PARK9-mediated lysosomal dysfunction and α-Syn accumulation in the pathogenesis of KRS (9).

However, these prior studies have not explained the possible linkages between deficiency of PARK9, increased sensitivity to metals, lysosomal dysfunction and α-Syn accumulation. To address these questions, we set out to perform an unbiased screening of various metals including manganese that was previously implicated in PARK9 function (7,8). These studies revealed that PARK9-depleted cells were most sensitive to Zn^{2+}. Increased concentration of Zn^{2+} resulted in impaired lysosomal proteolysis and increased expression of α-Syn. Together, these findings suggest that Zn^{2+} dyshomeostasis caused by loss of PARK9 contributes to PARK9-mediated lysosomal dysfunction and subsequent α-Syn accumulation.

RESULTS

PARK9 mutation increases sensitivity to extracellular zinc (Zn^{2+})

Recent studies have shown that PARK9-depleted yeast cells exhibit increased sensitivity to Mn^{2+} while over-expression of PARK9 was protective (7). Wild-type but not mutant PARK9 over-expression in HEK rendered cells resistant to Mn^{2+} toxicity (8). To further examine the relationship between PARK9 and metals, we performed an unbiased screening in fibroblasts carrying PARK9 mutation (MUT1 and MUT2) and wild-type controls (WT1 and WT2). After culturing the cells in medium in the presence of copper, iron, zinc, manganese or nickel for 24 h, we found that patient fibroblasts were most sensitive to Zn^{2+} (Fig. 1A). Using the Zn^{2+} chelator clioquinol (2 μM), we found that Zn^{2+} toxicity was greatly reduced (Fig. 1B). To confirm these findings in neurons, primary embryonic cortical neurons (PCNs) were transduced with lenti-shRNA targeting mouse *ATP13A2/PARK9* (PARK9 shRNA) or scrambled control shRNA (Scrb shRNA). We observed a significant reduction in PARK9 expression in PARK9-treated PCNs (Supplementary Material, Fig. S1). We found that 6 days post-infection (6 DPI), ATP13A2-depleted PCNs exhibited increased sensitivity to Zn^{2+}, whereas other cations did not exhibit a significant effect. Importantly, Zn^{2+} chelator, TPEN (*N*,*N*,*N*‘,*N*’-Tetrakis(2-pyridylmethyl)ethylenediamine) was able to attenuate Zn^{2+} toxicity in primary neurons (Fig. 1C and D, Supplementary Material, Fig. S2). Furthermore, loss of PARK9 did not alter the sensitivity of cells to increasing doses of Cu^{2+}, Fe^{2+}, Mn^{2+} and Ni^{2+} (Supplementary Material, Fig. S3). Taken together, these results show that the loss of PARK9 sensitized fibroblasts and neurons to Zn^{2+}, suggesting a protective role of PARK9 against increased concentrations of Zn^{2+}.

PARK9 mutation alters the intracellular distribution of Zn^{2+}

Previous immunocytochemical analyses have shown that exogenously expressed PARK9 colocalizes with acidic vesicles such as lysosomes (2,5,8) and that the loss of PARK9 results in lysosomal dysfunctions (10,11). However, the physiological function of PARK9 in lysosomes remains uncharacterized. Since Zn^{2+} normally accumulates in lysosomes (12,13), we asked whether PARK9 affects cellular distribution of Zn^{2+}. To this end, we stained WT and MUT fibroblasts with the Zn^{2+} probe FluoZin-3 together with LysoTracker Red that detects acidic vesicles. We found that most of the Zn^{2+} positive signal (green) colocalized with LysoTracker Red-positive vesicles in both WT and MUT fibroblasts (Fig. 2A). We (9) and others (11) have previously documented an increase in the area and number of LysoTracker Red-positive vesicles in MUT fibroblasts compared with WT fibroblasts probably due to a cellular compensatory response(Fig. 2A left panels and B left upper graph). The distribution of Zn^{2+}, as determined by FluoZin-positive puncta, was variable in each cells (Fig. 2A left panels and B left middle graph); however, when the Zn^{2+} positive green signal was normalized to the LysoTracker Red-positive signal, we found that the Zn^{2+} signal per vesicle was significantly decreased in MUT compared with WT fibroblasts (Fig. 2B left bottom graph), suggesting that PARK9-deficient acid vesicles contain less Zn^{2+} compared with wild-type acid vesicles. Next, we assessed how LysoTracker Red- and FluoZin-positive vesicles respond to increased extracellular Zn^{2+} (Zn^{2+} stress). After culturing the cells in the presence of 100 μM Zn^{2+} for 1 h, we found that the area of LysoTracker Red-positive vesicles is increased probably because vesicles sequestered excess cytosolic Zn^{2+} to prevent the toxic effects (Fig. 2A right panels and B right upper graph). Indeed, increased FluoZin fluorescence was observed in both WT and MUT fibroblasts (Fig. 2A right panels and B right middle graph). Interestingly, even under Zn^{2+} stress conditions, Zn^{2+} signal per vesicle was still significantly decreased in MUT compared with WT fibroblasts (Fig. 2B right bottom graph). These data suggest that PARK9-deficient acidic vesicles exhibit decreased capacity to sequester Zn^{2+} both under physiological conditions and under conditions of Zn^{2+} stress.

Loss of PARK9 induces the expression of zinc transporters and metalloproteins

Zn^{2+} concentration in the cytosol is tightly controlled by zinc transporters and metallothioneins (14). ZnT [solute-linked carrier 30 (SCL30)] family of transporters reduces cytosolic Zn^{2+} by releasing Zn^{2+} out of cells or into intracellular organelles (15), whereas metallothioneins sequester Zn^{2+} with multiple clusters of cysteine residues (16). Since the expressions of ZnT transporters and metalloproteins get induced by increased cytosolic Zn^{2+}, their expression can serve as an indicator of Zn^{2+} dyshomeostasis (17). To determine the levels of ZnT transporters in WT and MUT fibroblasts, real-time PCR was used to quantify expression levels of five zinc transporters, ZnT1, ZnT2, ZnT5, ZnT6 and ZnT7. While ZnT1 is mainly located on the plasma membrane, ZnT2, ZnT5, ZnT6 and ZnT7 localize to membranes of intracellular vesicles (18). We found that all zinc transporters tested were increased in MUT compared with WT fibroblasts (Fig. 3A). We then analyzed the expression of metallothionein-III (MT-III) that is exclusively expressed in neurons (19). As shown in Figure 3B, MT-III was significantly increased in PARK9-depleted primary neurons, further suggesting

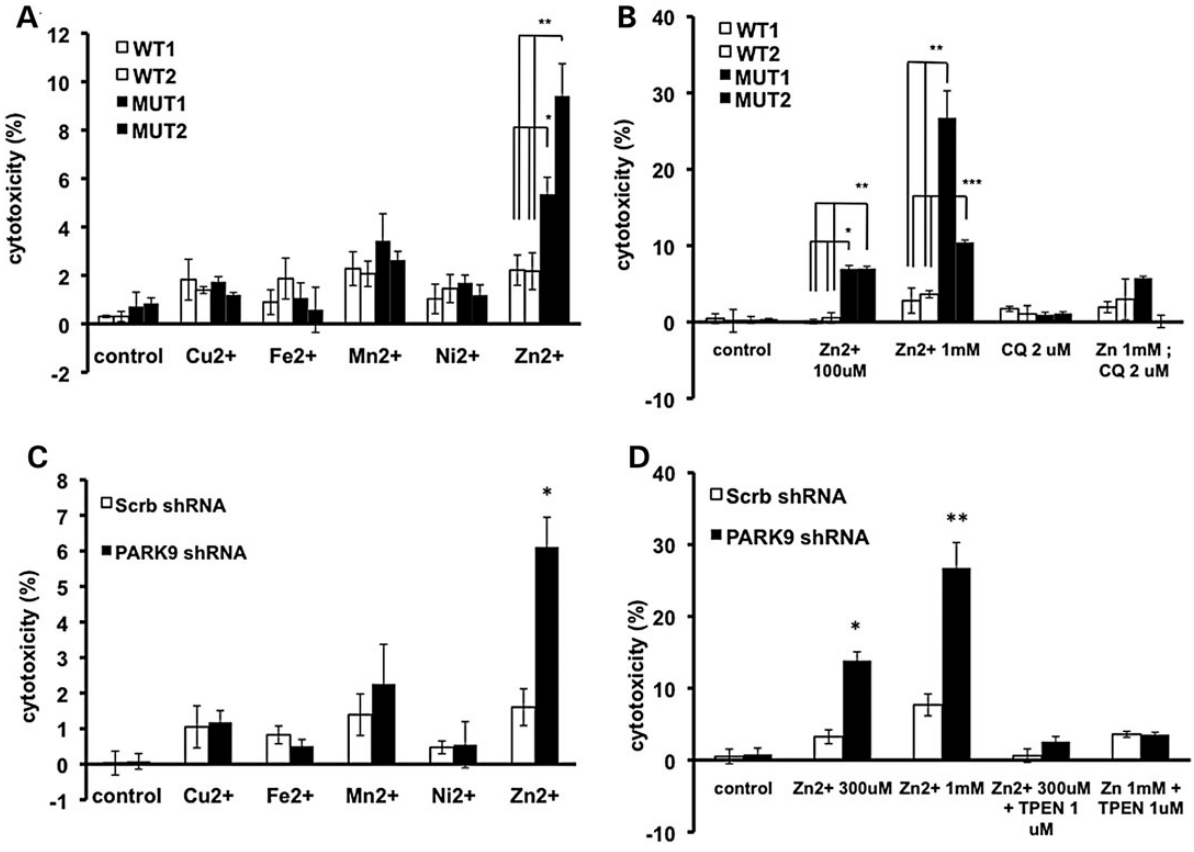

Figure 1. PARK9 mutant fibroblasts and primary cortical neurons are sensitive to zinc (Zn^{2+}). (**A**) LDH release from fibroblasts cultured in a medium containing one of the cations (Cu^{2+}, Fe^{2+}, Mn^{2+}, Ni^{2+} or Zn^{2+}, concentration is 100 μM) for 24 h ($n = 3$, $^{*}P < 0.005$, $^{**}P < 0.001$). (**B**) Toxicity of Zn^{2+} was attenuated by adding Zn^{2+} chelator, clioquinol (2 μM) in a medium ($n = 3$, $^{*}P < 0.01$, $^{**}P < 0.03$, $^{***}P < 0.001$). (**C**) LDH release from primary cortical neurons (PCN) cultured in the presence of cations ($n = 3$, $^{*}P < 0.005$). (**D**) Toxicity of Zn^{2+} was attenuated by adding Zn^{2+} chelator, TPEN (*N*,*N*,*N*‘,*N*’-Tetrakis(2-pyridylmethyl)ethylenediamine) (1 μM) ($n = 3$, $^{*}P < 0.05$, $^{**}P < 0.005$). The values are the mean ± SEM.

dyshomeostasis of Zn^{2+} and compensatory elevation of zinc transporters and metallothioneins in the presence of depleted PARK9. To examine whether expression of *PARK9* itself can be induced by Zn^{2+} stress, we treated primary neurons with 100 μM Zn^{2+}. Indeed, expression of *PARK9* was dramatically elevated in the presence of elevated Zn^{2+} (Fig. 3C), supporting the idea that PARK9 plays a role in regulating levels of cytosolic Zn^{2+}.

PARK9 expression affects zinc-mediated lysosomal dysfunction

Using a fluorescent Zn^{2+} probe, we showed a reduced accumulation of Zn^{2+} in acidic vesicles of patient fibroblasts (Fig. 2B). In addition, recent data established that deficiency of PARK9 resulted in impaired lysosomal proteolysis (9,11). Therefore, we asked whether Zn^{2+} mislocalization in mutant cells contributes to lysosomal dysfunction. To address this question, we performed long-lived protein degradation assay in primary neurons. We confirmed previous data that lysosomal proteolysis was reduced by PARK9 depletion (Fig. 4A and E). Moreover, we found that the presence of excessive Zn^{2+} impaired lysosomal proteolysis in primary neurons in a dose-dependent manner, an effect that was further worsened by depletion of PARK9 (Fig. 4E). Importantly, lentiviral transduction of PARK9 completely restored Zn^{2+}-mediated defect in lysosomal proteolysis (Fig. 4E). These data suggest that the loss of PARK9 renders lysosomes more vulnerable to Zn^{2+} stress, whereas expression of PARK9 protects from excessive neuronal Zn^{2+}. In light of the importance of maintaining low pH for the proper function of lysosomal acid hydrolases (20), we also examined the effect of excessive Zn^{2+} on lysosomal pH. As shown in Figure 4F, lysosomal pH was elevated in primary neurons by Zn^{2+} stress in a dose-dependent manner and exaggerated by PARK9 depletion, further emphasizing the protective role of PARK9 in Zn^{2+}-mediated lysosomal dysfunction.

Loss of PARK9 enhances Zn^{2+}-mediated α-Syn accumulation and impairs the function of lysosomal hydrolases

Previous studies showed that depletion of PARK9 led to the accumulation of α-Syn due to the decreased lysosomal function (9). Since our data demonstrated that elevated Zn^{2+} impairs lysosomal function, we wondered if α-Syn expression level was also increased by Zn^{2+} stress. As shown in Figure 5A, Zn^{2+} stress caused α-Syn accumulation in primary neurons and loss of PARK9 further enhanced Zn^{2+}-mediated α-Syn accumulation. Using an antibody to detect nitrated and oxidized

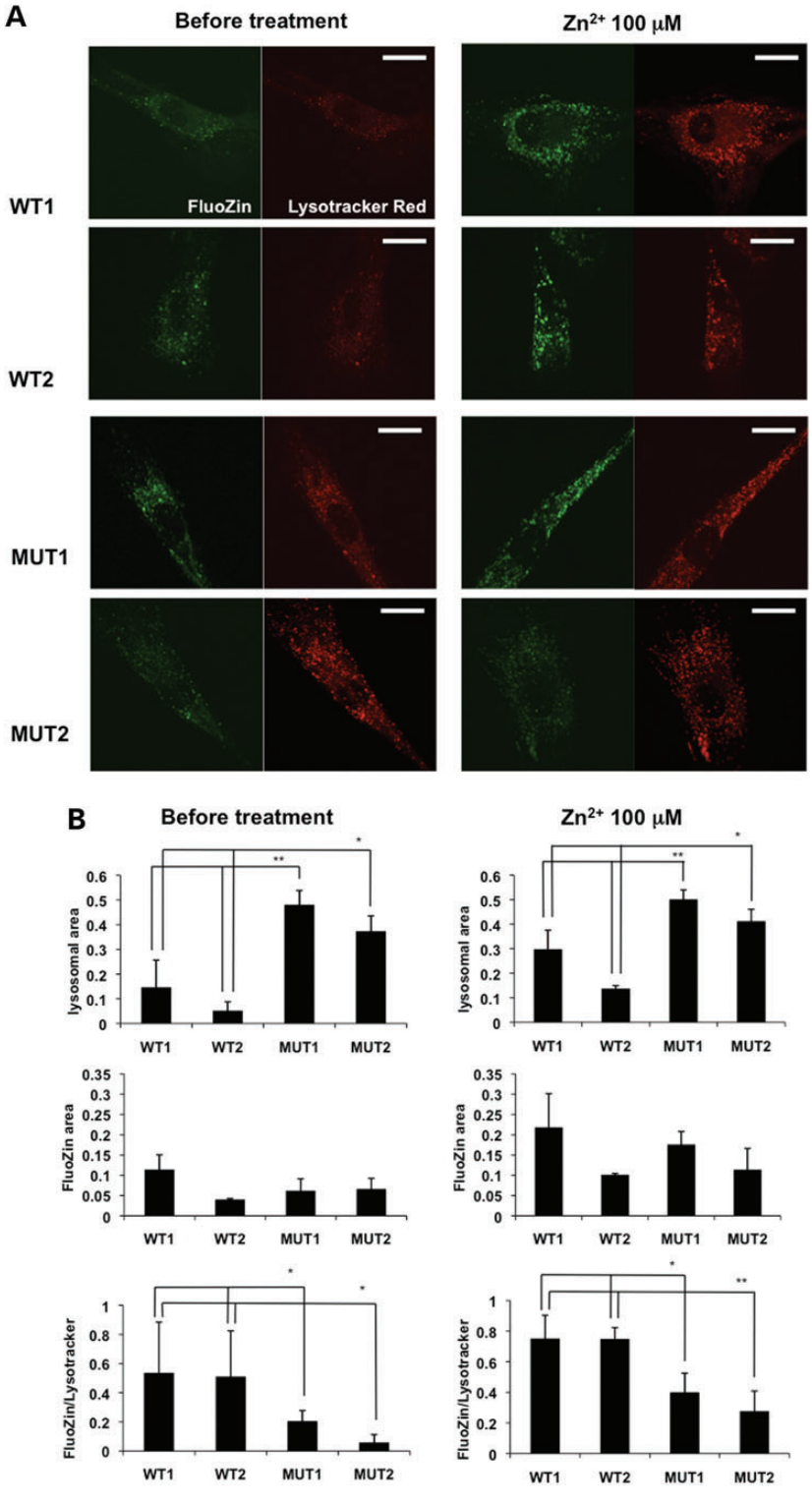

Figure 2. PARK9 mutation alters Zn^{2+} distribution in fibroblasts. (**A**) The representative confocal live-cell images of fibroblasts stained with FluoZin-3 (green) and LysoTracker Red (red). Two wild-type (WT1 and WT2) and two PARK9 mutant (MUT1 and MUT2) fibroblast lines were stained before (left) or after treatment with 100 μM Zn^{2+} for 1 h (right). Scale bars indicate 20 μm. (**B**) Quantification analysis of LysoTracker Red and FluoZin-3 area per total cell area before (left) and after Zn^{2+} incubation (right). Left, upper, quantification analysis of LysoTracker Red-positive area per total cell area ($n = 10$, $^{*}P < 0.01$, $^{**}P < 0.001$). Middle, quantification of FluoZin-3-positive area per total cell area ($n = 10$, $^{*}P < 0.005$). Bottom, quantification of FluoZin-3-positive area per LysoTracker Red-positive area ($n = 10$, $^{*}P < 0.05$). Right, upper, quantification of LysoTracker Red-positive area per total cell area ($n = 10$, $^{*}P < 0.05$, $^{**}P < 0.03$). Middle, quantification of FluoZin-3-positive area per total cell area. Bottom, quantification analysis of FluoZin-3-positive area per LysoTracker Red-positive area ($n = 10$, $^{*}P < 0.03$, $^{**}P < 0.005$). The values are the mean ± SEM.

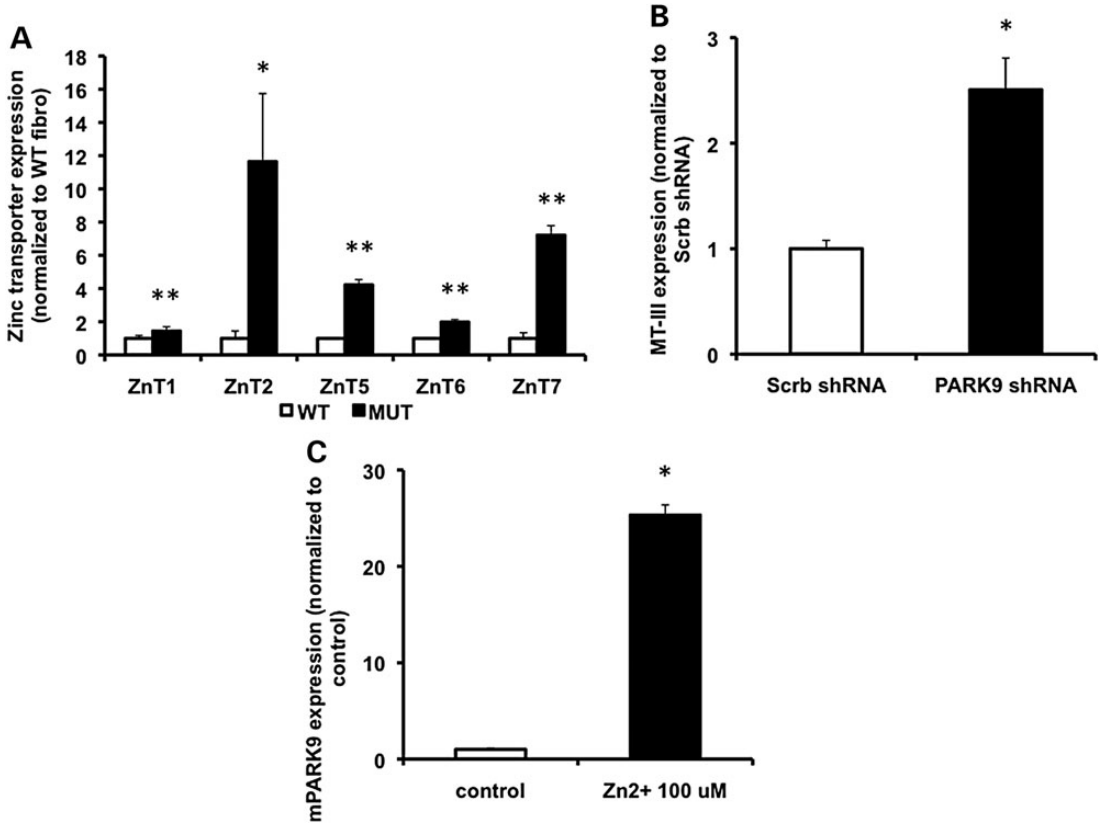

Figure 3. Loss of PARK9 induces expression of zinc transporters and metallothionein proteins. (**A**) The mRNA expression of indicated zinc transporters in WT and MUT fibroblasts ($n = 3$, $^{*}P < 0.05$, $^{**}P < 0.03$). The expression of zinc transporters in MUT fibroblasts is divided by that in WT fibroblasts. (**B**) The mRNA expression of *MT-III* in scrambled- (Scrb) and PARK9 shRNA-treated primary cortical neurons (PCNs) ($n = 3$, $^{*}P < 0.001$). The expression of *MT-III* in PARK9-treated PCNs is divided by that in Scrb-treated PCNs. (**C**) The *PARK9* mRNA expression in PCNs cultured in the presence of 100 μM Zn^{2+} ($n = 3$, $^{*}P < 0.001$). The expression of *PARK9* in PCNs cultured the medium containing 100 μM Zn^{2+} is divided by that in PCNs cultured the normal medium. The values are the mean ± SEM.

α-Syn (syn 505), we found an increase in oxidized high molecular weight species of α-Syn upon Zn^{2+} stress, suggesting that Zn^{2+} stress may lead to oxidation and oligomerization of α-Syn. Depletion of PARK9 further increased nitrated/oxidized α-Syn oligomers, indicating a possible protective role of PARK9 in conditions of Zn^{2+}-mediated oxidative stress.

We have previously shown that increased levels of α-Syn impaired intracellular trafficking of lysosomal glucocerebrosidase (GCase) from endoplasmic reticulum-to-Golgi (21). To examine if Zn^{2+}-mediated α-Syn accumulation also affects GCase activity, we examined lysosome-enriched fractions of primary neurons for GCase activity. As shown in Figure 5B, GCase activity was significantly decreased upon Zn stress and/or PARK9 depletion. These results suggest that PARK9 deficiency and dyshomeostasis of Zn^{2+} generate a pathological loop that leads to deficient trafficking of lysosomal GCase and further impairment of lysosomal function.

In order to more directly examine the effect of Zn^{2+} dyshomeostasis on lysosomal function, we examined lysosomal acid sphingomyelinase (L-SMase), an important lysosomal hydrolase that has been linked to Niemann-Pick disease (22). A mature form of L-SMase is processed from a pro-enzyme in a zinc-dependent manner (23). We found that L-SMase activity was significantly reduced in PARK9-deficient cells compared with wild-type cells (Fig. 5C), suggesting that a decrease in L-SMase activity may represent at least one mechanism of Zinc-mediated lysosomal dysfunction in models of KRS.

DISCUSSION

Zinc is the second most abundant trace element in the human body after iron (24), and potentially affects the structure and activity of ∼10% of proteins (25), including more than 300 enzymes (26). Zinc has an important role in gene expression by binding transcriptional activators (17) and also functions as a signaling mediator, such as a cell-to-cell communication and an intracellular signaling (14).

Zn^{2+} dyshomeostasis has been associated with a variety of neurological disorders from ischemia to neurodegeneration (27). In Alzheimer's disease (AD), high levels of zinc are found in the cortex (28) and zinc enhances amyloid-β aggregation that is a pathological hallmark of AD (29). Similarly, zinc is increased in SN (30,31) and cerebrospinal fluid (32) in PD, indicating a possible involvement in PD pathogenesis. Here, we provide evidence that Zn^{2+} dyshomeostasis is also linked to KRS, a rare form of hereditary parkinsonism and dementia.

Zinc ions are hydrophilic and thus do not cross the plasma membrane by passive diffusion, but rather zinc transporters are required (15). Intracellular zinc is primarily coupled with

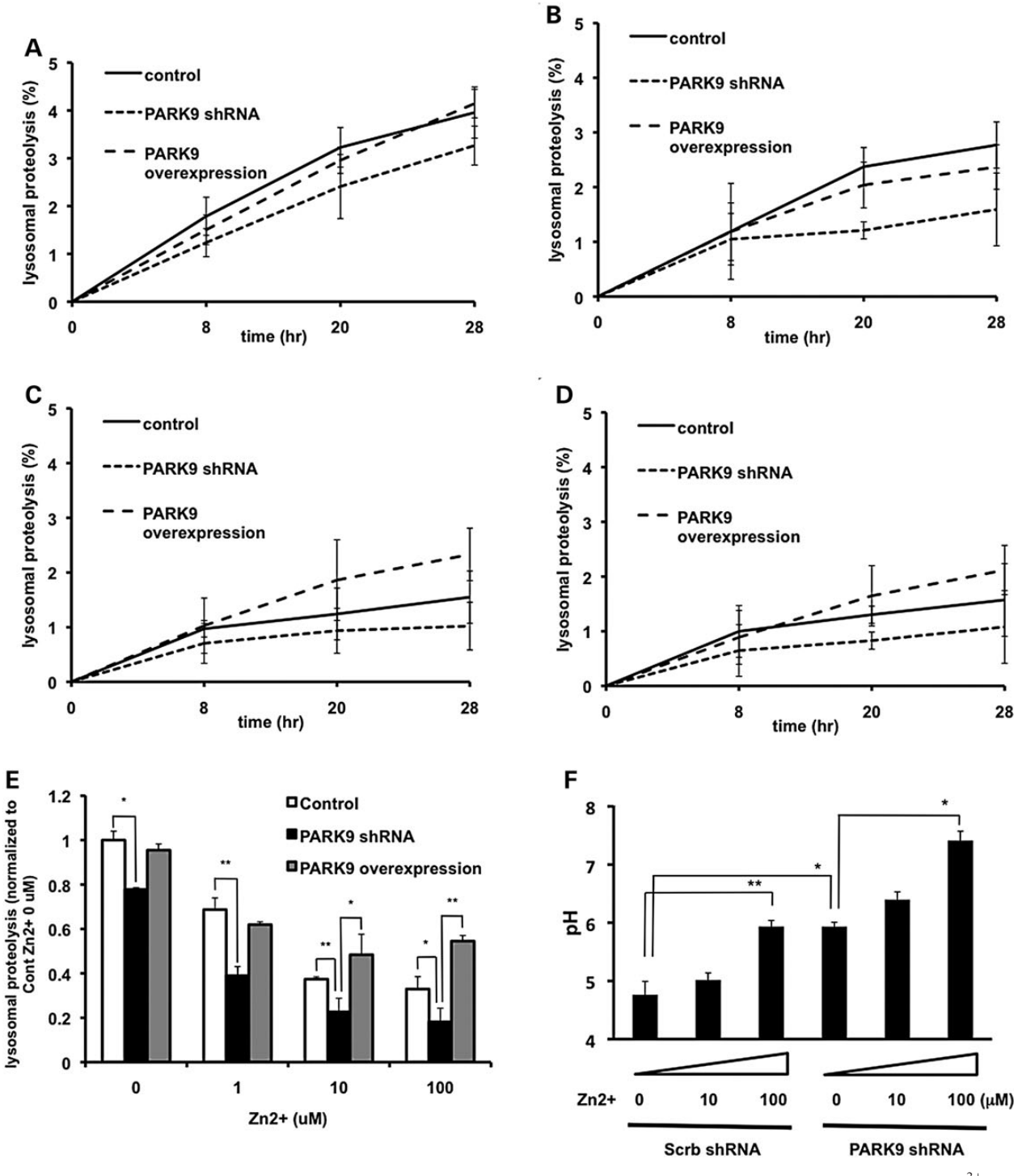

Figure 4. Zinc dyshomeostasis leads to impaired lysosomal function. (**A**–**E**) PARK9 expression affects lysosomal proteolysis that is impaired by Zn^{2+}. Lysosomal proteolysis in control, PARK9-depleted or PARK9 over-expressed PCNs cultured in a medium containing either 0 μM (A), 1 μM (B), 10 μM (C) or 100 μM Zn^{2+} (D). Lysosomal proteolysis is calculated by subtracting lysosomal inhibitors (2.5 mM NH_4Cl and 50 μM leupeptin) sensitive proteolysis from total proteolysis at 8, 20 and 28 h after chase. (**E**) Quantification of lysosomal proteolysis is calculated from the area under the curve ($n = 3$, $^{*}P < 0.05$, $^{**}P < 0.005$). (**F**) Dual-emission ratiometric measurement of lysosomal pH using LysoSensor Yellow/Blue DND-160. The effect of Zn^{2+} on lysosomal pH in Scrb or PARK9 shRNA treated PCNs is shown ($n = 3$, $^{*}P < 0.05$, $^{**}P < 0.005$). The values are the mean ± SEM.

proteins or DNA and only small amounts of zinc exist in free form (33). It is therefore important that the concentration of cytosolic Zn^{2+} is tightly regulated to avoid toxicity. It has been well established that zinc transporters and Zn^{2+} permeable channels, as well as zinc buffering proteins such as MTs regulate levels of cytosolic zinc (14). Using fluorescent zinc probes to track dynamic movement of zinc, it was revealed that intracellular organelles such as lysosomes store zinc in a wide variety of

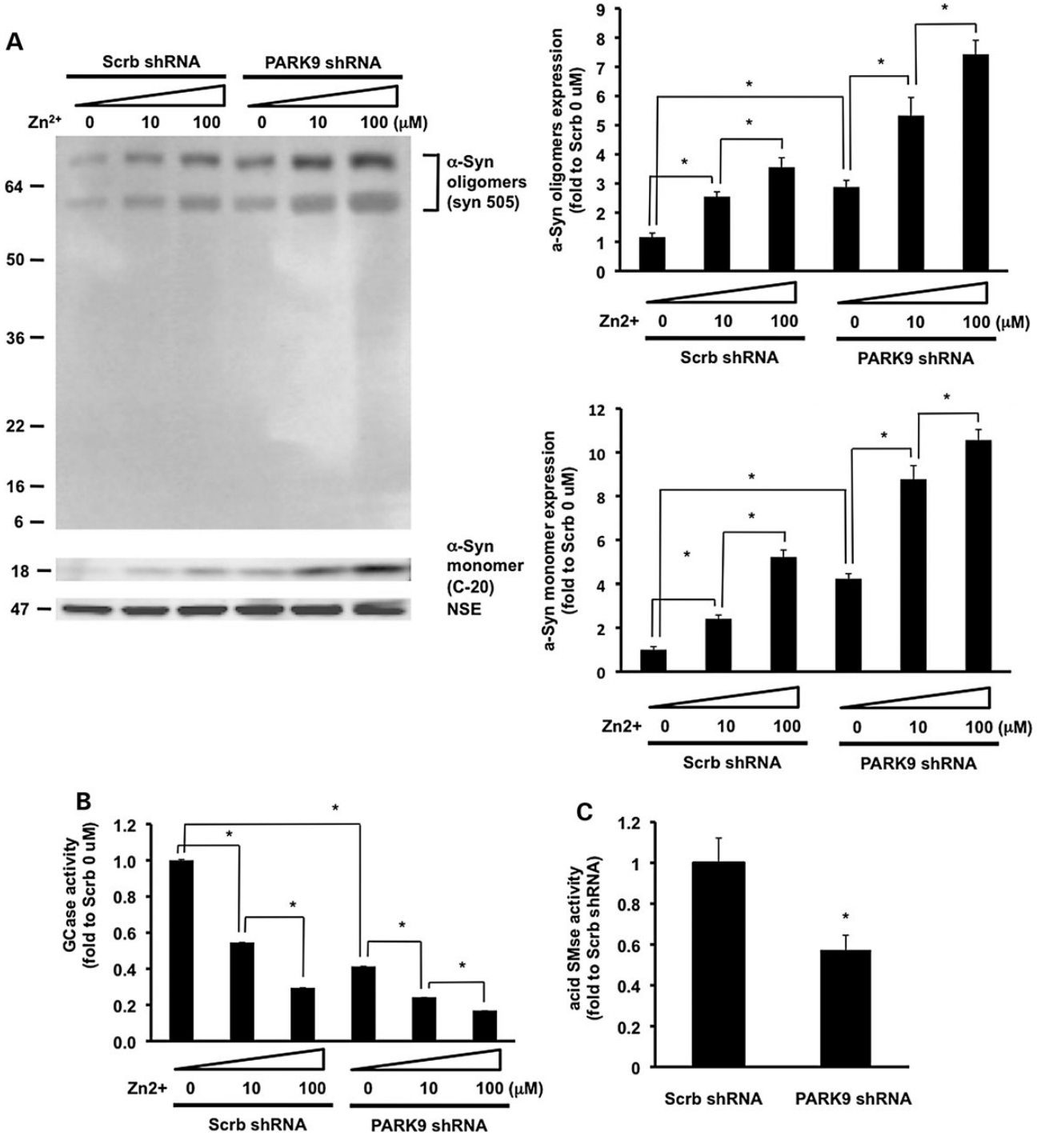

Figure 5. Loss of PARK9 enhances zinc-mediated α-Syn accumulation and reduction of lysosomal hydrolases activities. (**A**) Upper left: western blot analysis of the effect of Zn^{2+} on α-Syn expression in PCNs treated with Scrb or PARK9 shRNA. NSE was used as loading control. MW is shown as kDa. Bottom left: the results of densitometric analysis of α-Syn oligomers which were detected with syn 505 ($^*P < 0.01$). Upper right: the results of densitometric analysis of α-Syn monomers which were detected with C-20 ($^*P < 0.01$). (**B**) Glucocerebrosidase (GCase) activities in lysosome-enriched fractions extracted from PCNs ($n = 3$, $^*P < 0.005$). (**C**) Acid sphingomyelinase (aSMase) activities in lysosome-enriched fractions extracted from PCNs ($n = 3$, $^*P < 0.03$).

species, from yeast *Saccharomyces cerevisiae* (34), *Caenorhabditis elegance*, (35), to mammalian cells (36). To maintain low cytosolic concentration, excessive Zn^{2+} is rapidly sequestered into lysosomes (12,37). In neurons, Zn^{2+} is also sequestered in presynaptic vesicles, released in neuronal activity-dependent manner and taken into postsynaptic vesicles through Ca^{2+} channels, 2-amino-3-(3-hydroxy-5-methylisoxazol-4-yl) propanoic acid and other receptors (27,33).

Our data suggest that PARK9-deficient lysosomes exhibit a decreased capacity to store Zn^{2+} (Fig. 2), possibly due to loss

of PARK9-mediated Zn^{2+} import from cytosol into vesicles. While it is difficult to detect low levels of free cytosolic zinc with the current technology, levels of zinc transporters and metallothioneins can serve as indirect indicators of zinc dyshomeostasis due to their responsiveness to cytosolic Zn^{2+} (17). Early studies in *Escherichia coli* revealed that extremely low cytosolic Zn^{2+} (femtomollar) is sufficient for induction of these proteins (38), whereas studies in mammalian cells have been more challenging due to high vesicular and very low cytosolic Zn^{2+}. There is accumulating evidence that the induction of zinc transporters alters zinc homeostasis (39). Among all zinc transporters, the best-characterized transporters are ZnT1 and ZnT2. While ZnT1 is expressed in the plasma membrane, ZnT2 is expressed in vesicular membranes. The mRNA and protein expression of these transporters are induced by zinc exposure (40,41). ZnT1-deficient cells exhibit increased intracellular Zn^{2+} due to low zinc efflux, while over-expression of ZnT1 leads to reduced zinc concentration by increasing zinc efflux (42). Similarly, ZnT2 deficient cells have less vesicular Zn^{2+}, whereas over-expression of ZnT2 results in accumulation of Zn^{2+} in acidic vesicles (36). These results suggest that induction of zinc transporters correlates with reduction of cytosolic Zn^{2+}. We found that zinc transporters and MT-III were increased in PARK9 mutant cells (Fig. 3), indicating increased cytosolic Zn^{2+} in PARK9-deficient cells. We also found that expression of wild-type PARK9 is induced by high Zn^{2+}, corroborating the role of PARK9 in Zn^{2+} homeostasis (Fig. 3). Interestingly, both PARK9 mRNA and zinc are increased in postmortem brains from sporadic PD patients (2,5,30,31), suggesting that zinc may contribute to upregulation of PARK9 *in vivo*. However, the contribution of PARK9 and zinc to sporadic PD will require further study.

Since Zn is not involved in redox reactions like Fe^{2+} or Cu^{2+}, it does not generate oxidative stress by itself (24). However, elevated levels of Zn^{2+} inhibit mitochondrial function via inhibition of α-ketoglukarate dehydrogenase in TCA cycle (43) or bc_1 complex in complex III (44), or via induction of mitochondrial membrane permeability (45). These effects on mitochondria may consequently generate reactive oxygen species (ROS) (46). To this end, mitochondrial damage accompanied by abnormal production of ROS and decreased ATP synthesis has been reported in PARK9 mutant cells (47,48). As shown in the accompanying manuscript by Park *et al*., insufficient sequestration of Zn^{2+} into intracellular vesicles in PARK9-deficient cells leads to mitochondrial dysfunction and induction of ROS. Moreover, they and others have also demonstrated increased mitochondrial fragmentation in the presence of mutant PARK9, suggesting an impairment of mitochondrial clearance, possibly due to insufficient lysosomal degradation (5,48).

Our previous work (9,49), as well as the work by another group (11), showed that lysosomal dysfunction in PARK9-deficient cells and mice resulted in the accumulation of α-Syn. Genetic studies revealed a dosage relationship between α-Syn and severity of PD (50), indicating that the expression level of α-Syn significantly contributes to disease pathogenesis in PD and other related synucleinopathies. Here, we found that the expression level of α-Syn was increased upon Zn^{2+} stress in primary neurons (Fig. 5A). Since lysosomal proteolysis is impaired by Zn^{2+} stress (Fig. 3), accumulation of α-Syn is likely due to reduced lysosomal degradation. In addition to increased monomeric α-Syn, we found elevated nitrated/oxidized oligomeric α-Syn in the presence of elevated neuronal Zn^{2+} (Fig. 5A). Previous studies suggest that mitochondria-driven oxidative stress can induce α-Syn oligomerization (51), and that aggregation of α-Syn is reduced by attenuating oxidative stress (52). Therefore, we hypothesized that increased oxidative stress may also contribute to Zn^{2+}-induced α-Syn oligomerization.

Our results suggest that decreased uptake of zinc into lysosomes and increased cytosolic zinc contributes to lysosomal dysfunction. In order to explain how Zn^{2+} dyshomeostasis impairs lysosomal proteolysis, we considered the following possibilities. First, we found elevation of lysosomal pH in the presence of high neuronal zinc (Fig. 4F). Lysosomal pH is mainly regulated by cations/anions that move across the lysosomal membrane and is necessary to dissipate transmembrane voltage created by the activity of vacuolar ATPase (20). Although it has been known that Cl^- and K+ are involved in the process (20), the precise mechanism of voltage dissipation remains largely undetermined. Further studies will be required to clarify the role of PARK9 and Zn^{2+} in this process.

Second, recent evidence suggests that accumulated α-Syn impairs lysosomal function indirectly via its effects on trafficking of lysosomal hydrolases (21) or via lysosomal rupture (53). In our previous work, we showed that trafficking of lysosomal GCase is impaired in the presence of increased α-Syn (21), which in turn contributed to decreased lysosomal degradation capacity. Here, we showed that Zn^{2+} stress reduced GCase activity in lysosome-enriched neuronal fractions. Since elevated Zn^{2+} stress also resulted in increased levels of α-Syn, we hypothesized that Zn^{2+} inhibits trafficking of GCase via increased α-Syn, which creates a pathogenic loop (Fig. 5A and B). While more work will be required to elucidate the details of this mechanism, our data suggest that PARK9 and GCase may be mechanistically linked via α-Syn accumulation in the pathogenesis of synucleinopathies.

Finally, we found that decreased lysosomal zinc in PARK9-deficient cells resulted in reduced activity of lysosomal acid sphingomyelinase (aSMase), an important lysosomal hydrolase. Prior studies suggested that maturation of pro-aSMase to L-SMase requires Zn^{2+} (54). Therefore, we hypothesized that Zn^2 deficiency in PARK9 lysosomes may inhibit this important maturation step. As shown in Figure 5C, aSMase activity was reduced in lysosome-enriched fractions isolated from PARK9 primary neurons (Fig. 5C). These results together with studies in aSMase-deficient mice that exhibit severe lysosomal pathology (55) suggest that Zn^{2+} deficiency in lysosomes contributes PARK9-mediated lysosomal dysfunction.

Together, our findings highlight the importance of PARK9 in regulating zinc homeostasis and lysosomal function. It will be of interest to examine if targeting zinc may prove beneficial as a novel treatment approach for KRS and related synucleinopathies.

MATERIALS AND METHODS

Plasmids

Lentiviral plasmids expressing short hairpin plasmid RNA (shRNA) targeting mouse *Atp13a2* and scrambled control were used for viral packaging (9). Human lenti-PARK9 was a

gift from Chris Rochet. The virus titers were calculated using HIV-1 p24 Antigen ELISA kit (Zeptometrix).

Cell culture

Primary dermal fibroblasts carrying a homozygous mutation (1550C>T) (MUT1) and compound heterozygous mutations (3176 T>G, 3253 delC) (MUT2) in PARK9 were generously provided by Christine Klein and Carolyn Sue, respectively. Fibroblasts and mouse embryonic cortical neurons were cultured as described in references (9) and (56), respectively. Neurons were infected at a multiplicity of infection of 1 at day *in vitro* 4, and harvested at 6 DPI. The cytotoxicity of Zn^{2+} to fibroblasts and primary cortical neurons were evaluated by release of lactate dehydrogenase (LDH), following the manufacturer's protocol (CytoTox 96 Non-Radioactive Cytotoxicity Assay, Promega). Cytotoxicity was calculated, as follows: cytotoxicity (%) = (test sample − sample for spontaneous LDH release)/(sample for maximum LDH release − sample for spontaneous LDH release).

Live-cell confocal imaging

Fibroblasts were seeded in Lab-Tek glass-bottom chamber slides (Nunc) and incubated with FluoZin™-3, Lysotracker® Red DND-99 and Hoechst33342 (NucBlue™ Live Cell Stain, Invitrogen) for 30 min. Live-cell imaging was conducted on the Zeiss LSM 510 meta confocal system with an inverted Zeiss Axiovert 200 M microscope equipped with a EC Paln Neofluar ×100 (1.3 numerical aperture) oil immersion objective. FluoZin™-3 was excited with an Argon laser at 488 nm, and emission was detected with a band-pass filter of 500–530 nm. Lysotracker Red was excited with a helium-neon laser at 543 nm, and emission was detected with a band-pass filter of 565–615 nm. DAPI was excited with Ti: sapphire tunable laser (Chameleon, Coherent) at 750 nm, and emission was detected with a band-pass filter of 435–485 nm. Images were collected using Zeiss LSM 3.5 software and exported as JPEG images for analysis using Image J software.

RNA extract and real-time PCR

Total RNA was extracted from fibroblasts or primary neurons at 6 DPI using RNeasy Mini (Qiagen) with DNase treatment (Qiagen). The total content of RNA was measured using a NanoDrop (Thermo). Reverse transcription was performed using SuperScript III First-Strand Synthesis SuperMix (Invitrogen). Real-time PCR was conducted using a SYBR Green ER SuperMix (Invitrogen). Signals from SYBR Green were recorded and analyzed by the iCycler Real-Time PCR System (Bio-Rad, USA). β-Actin was used as an internal control.

Proteolysis of long-lived proteins

Long-lived protein degradation assay was performed as previously described (21). Briefly, primary cortical neurons were plated in 12-well dishes at the density of 50 000/well. The culture medium was changed to the medium containing [3H]leucine (hot medium) 48 h before chasing. For lysosomal inhibition, 50 μM of leupeptin was added to the hot medium and 50 μM of leupeptin and 5 μM of NH_4Cl are added to the chasing medium. From the 700 μl of chasing medium, 70 μl of medium was collected at 8, 20 and 28 h after chasing, and precipitated with TCA (final conc: 10%) and albumin (0.15 mg/ml) for at 4°C for 16 h followed by centrifugation at 20 000 rcf for 25 min. Radioactivities of soluble fractions were measured using liquid scintillation system (LS 1701, Beckman).

Lysosomal pH

Cells were plated in 96-well plates at the density of 50 000/well. After staining with LysoSensor™ Yellow/Blue DND-160 (1 mM; Invitrogen), fluorescence was measured with a fluorescence plate reader (VICTOR2, Perkin-Elmer). To obtain a calibration curve, cells were equilibrated with MES buffers with the pH adjusted to 3.5 to 8.0 along with 10 μM nigericin and 10 μM monensin for 5 min before staining with LysoSensor. A standard curve was made to plot the fluorescence ratio ($Yellow^{535}$/$Blue^{460}$) against the pH of MES buffers.

Western blotting

Western blotting was conducted as previously described with a few modifications (57). Briefly, mouse embryonic cortical neurons were harvested and lysed in a RIPA buffer (50 mM Tries pH 7.4, 150 mM Nail, 0.1% SDS, 0.5% Na deoxycholate, 1% NP-40) with protease inhibitor (Roche). We loaded 15 μg of homogenized proteins per lane. After running 8–16% Tris-Glycine gels, the samples were transferred to PVDF membranes (Millipore), which were blocked in PBS with 5% milk and 0.1% Tween20 (blocking buffer) at room temperature for 1 h, followed by incubation with α-Syn antibodies (syn 505; Invitrogen, C-20; Santa Cruz) or neural-specific enolase (NSE) antibody (#16625; Polysciences, Inc) in a blocking buffer at 4°C overnight. After incubated with appropriate secondary antibodies, the membranes were scanned with the Odyssey Infrared Imaging System (LiCor Biosciences).

Glucocerebrosidase and acid sphingomyelinase activity assays

GCase activity assay was performed as described (21). Briefly, lysosome-enriched P2 fractions were extracted from the primary neurons treated with scrambled (Scrb) shRNA or PARK9 shRNA and then resuspended in activity assay buffer. Fluorescence was measured after incubating with 1 mM 4-methylumbelliferyl β-glucophyranoside for 40 min. Acid sphingomyelinase activity was measured following the manufacture's instruction (Sphingomyelinase Fluorometric Assay Kit, Cayman Chemical).

Statistical analysis

All data were prepared for analysis with standard spreadsheet software (Microsoft Excel). All errors bars shown in the figures are SEM.

SUPPLEMENTARY MATERIAL

Supplementary Material is available at *HMG* online.

ACKNOWLEDGEMENTS

We thank all the members of Krainc laboratory for helpful suggestions and critical discussion. We also thank Chris Rochet and Josephat Asiago for human *PARK9* expression construct, and to Carolyn Sue and Christine Klein for human dermal fibroblasts.

Conflict of Interest statement. None declared.

FUNDING

This work was supported by National Institute of Health (R01NS076054 to D.K.).

REFERENCES

1. Najim al-Din, A.S., Wriekat, A., Mubaidin, A., Dasouki, M. and Hiari, M. (1994) Pallido-pyramidal degeneration, supranuclear upgaze paresis and dementia: Kufor-Rakeb syndrome. *Acta Neurol. Scand.*, **89**, 347–352.
2. Ramirez, A., Heimbach, A., Grundemann, J., Stiller, B., Hampshire, D., Cid, L.P., Goebel, I., Mubaidin, A.F., Wriekat, A.L., Roeper, J. *et al.* (2006) Hereditary parkinsonism with dementia is caused by mutations in ATP13A2, encoding a lysosomal type 5 P-type ATPase. *Nat. Genet.*, **38**, 1184–1191.
3. Park, J.S., Mehta, P., Cooper, A.A., Veivers, D., Heimbach, A., Stiller, B., Kubisch, C., Fung, V.S., Krainc, D., Mackay-Sim, A. *et al.* (2011) Pathogenic effects of novel mutations in the P-type ATPase ATP13A2 (PARK9) causing Kufor-Rakeb syndrome, a form of early-onset parkinsonism. *Hum. Mutat.*, **32**, 956–964.
4. Podhajska, A., Musso, A., Trancikova, A., Stafa, K., Moser, R., Sonnay, S., Glauser, L. and Moore, D.J. (2012) Common pathogenic effects of missense mutations in the P-type ATPase ATP13A2 (PARK9) associated with early-onset parkinsonism. *PLoS ONE*, **7**, e39942.
5. Ramonet, D., Podhajska, A., Stafa, K., Sonnay, S., Trancikova, A., Tsika, E., Pletnikova, O., Troncoso, J.C., Glauser, L. and Moore, D.J. (2012) PARK9-associated ATP13A2 localizes to intracellular acidic vesicles and regulates cation homeostasis and neuronal integrity. *Hum. Mol. Genet.*, **21**, 1725–1743.
6. Axelsen, K.B. and Palmgren, M.G. (1998) Evolution of substrate specificities in the P-type ATPase superfamily. *J. Mol. Evol.*, **46**, 84–101.
7. Gitler, A.D., Chesi, A., Geddie, M.L., Strathearn, K.E., Hamamichi, S., Hill, K.J., Caldwell, K.A., Caldwell, G.A., Cooper, A.A., Rochet, J.C. *et al.* (2009) Alpha-synuclein is part of a diverse and highly conserved interaction network that includes PARK9 and manganese toxicity. *Nat. Genet.*, **41**, 308–315.
8. Tan, J., Zhang, T., Jiang, L., Chi, J., Hu, D., Pan, Q., Wang, D. and Zhang, Z. (2011) Regulation of intracellular manganese homeostasis by Kufor-Rakeb syndrome-associated ATP13A2 protein. *J. Biol. Chem.*, **286**, 29654–29662.
9. Usenovic, M., Tresse, E., Mazzulli, J.R., Taylor, J.P. and Krainc, D. (2012) Deficiency of ATP13A2 leads to lysosomal dysfunction, alpha-synuclein accumulation, and neurotoxicity. *J. Neurosci.*, **32**, 4240–4246.
10. Usenovic, M. and Krainc, D. (2012) Lysosomal dysfunction in neurodegeneration: the role of ATP13A2/PARK9. *Autophagy*, **8**, 987–988.
11. Dehay, B., Ramirez, A., Martinez-Vicente, M., Perier, C., Canron, M.H., Doudnikoff, E., Vital, A., Vila, M., Klein, C. and Bezard, E. (2012) Loss of P-type ATPase ATP13A2/PARK9 function induces general lysosomal deficiency and leads to Parkinson disease neurodegeneration. *Proc. Natl Acad. Sci. USA*, **109**, 9611–9616.
12. Hwang, J.J., Lee, S.J., Kim, T.Y., Cho, J.H. and Koh, J.Y. (2008) Zinc and 4-hydroxy-2-nonenal mediate lysosomal membrane permeabilization induced by H2O2 in cultured hippocampal neurons. *J. Neurosci.*, **28**, 3114–3122.
13. Varea, E., Alonso-Llosa, G., Molowny, A., Lopez-Garcia, C. and Ponsoda, X. (2006) Capture of extracellular zinc ions by astrocytes. *Glia*, **54**, 304–315.
14. Fukada, T., Yamasaki, S., Nishida, K., Murakami, M. and Hirano, T. (2011) Zinc homeostasis and signaling in health and diseases: Zinc signaling. *J. Biol. Inorg. Chem.*, **16**, 1123–1134.
15. Liuzzi, J.P. and Cousins, R.J. (2004) Mammalian zinc transporters. *Annu. Rev. Nutr.*, **24**, 151–172.
16. Vasak, M. and Meloni, G. (2011) Chemistry and biology of mammalian metallothioneins. *J. Biol. Inorg. Chem.*, **16**, 1067–1078.
17. Jackson, K.A., Valentine, R.A., Coneyworth, L.J., Mathers, J.C. and Ford, D. (2008) Mechanisms of mammalian zinc-regulated gene expression. *Biochem. Soc. Trans.*, **36**, 1262–1266.
18. Kambe, T., Yamaguchi-Iwai, Y., Sasaki, R. and Nagao, M. (2004) Overview of mammalian zinc transporters. *Cell. Mol. Life Sci.*, **61**, 49–68.
19. Palmiter, R.D., Findley, S.D., Whitmore, T.E. and Durnam, D.M. (1992) MT-III, a brain-specific member of the metallothionein gene family. *Proc. Natl Acad. Sci. USA*, **89**, 6333–6337.
20. Mindell, J.A. (2012) Lysosomal acidification mechanisms. *Annu. Rev. Physiol.*, **74**, 69–86.
21. Mazzulli, J.R., Xu, Y.H., Sun, Y., Knight, A.L., McLean, P.J., Caldwell, G.A., Sidransky, E., Grabowski, G.A. and Krainc, D. (2011) Gaucher disease glucocerebrosidase and alpha-synuclein form a bidirectional pathogenic loop in synucleinopathies. *Cell*, **146**, 37–52.
22. Schulze, H. and Sandhoff, K. (2011) Lysosomal lipid storage diseases. *Cold Spring Harb. Perspect. Biol.*, **3**, a004804.
23. Jenkins, R.W., Idkowiak-Baldys, J., Simbari, F., Canals, D., Roddy, P., Riner, C.D., Clarke, C.J. and Hannun, Y.A. (2011) A novel mechanism of lysosomal acid sphingomyelinase maturation: requirement for carboxyl-terminal proteolytic processing. *J. Biol. Chem.*, **286**, 3777–3788.
24. Tapiero, H. and Tew, K.D. (2003) Trace elements in human physiology and pathology: zinc and metallothioneins. *Biomed. Pharmacother.*, **57**, 399–411.
25. Andreini, C., Banci, L., Bertini, I. and Rosato, A. (2006) Counting the zinc-proteins encoded in the human genome. *J. Proteome Res.*, **5**, 196–201.
26. Vallee, B.L. and Auld, D.S. (1990) Zinc coordination, function, and structure of zinc enzymes and other proteins. *Biochemistry*, **29**, 5647–5659.
27. Sensi, S.L., Paoletti, P., Bush, A.I. and Sekler, I. (2009) Zinc in the physiology and pathology of the CNS. *Nat. Rev. Neurosci.*, **10**, 780–791.
28. Religa, D., Strozyk, D., Cherny, R.A., Volitakis, I., Haroutunian, V., Winblad, B., Naslund, J. and Bush, A.I. (2006) Elevated cortical zinc in Alzheimer disease. *Neurology*, **67**, 69–75.
29. Bush, A.I., Pettingell, W.H., Multhaup, G., d Paradis, M., Vonsattel, J.P., Gusella, J.F., Beyreuther, K., Masters, C.L. and Tanzi, R.E. (1994) Rapid induction of Alzheimer A beta amyloid formation by zinc. *Science*, **265**, 1464–1467.
30. Dexter, D.T., Jenner, P., Schapira, A.H. and Marsden, C.D. (1992) Alterations in levels of iron, ferritin, and other trace metals in neurodegenerative diseases affecting the basal ganglia. The Royal Kings and Queens Parkinson's Disease Research Group. *Ann. Neurol.*, **32** (suppl.), S94–S100.
31. Dexter, D.T., Carayon, A., Javoy-Agid, F., Agid, Y., Wells, F.R., Daniel, S.E., Lees, A.J., Jenner, P. and Marsden, C.D. (1991) Alterations in the levels of iron, ferritin and other trace metals in Parkinson's disease and other neurodegenerative diseases affecting the basal ganglia. *Brain*, **114**(Pt 4), 1953–1975.
32. Hozumi, I., Hasegawa, T., Honda, A., Ozawa, K., Hayashi, Y., Hashimoto, K., Yamada, M., Koumura, A., Sakurai, T., Kimura, A. *et al.* (2011) Patterns of levels of biological metals in CSF differ among neurodegenerative diseases. *J. Neurol. Sci.*, **303**, 95–99.
33. Frederickson, C.J., Koh, J.Y. and Bush, A.I. (2005) The neurobiology of zinc in health and disease. *Nat. Rev. Neurosci.*, **6**, 449–462.
34. Devirgiliis, C., Murgia, C., Danscher, G. and Perozzi, G. (2004) Exchangeable zinc ions transiently accumulate in a vesicular compartment in the yeast Saccharomyces cerevisiae. *Biochem. Biophys. Res. Commun.*, **323**, 58–64.
35. Roh, H.C., Collier, S., Guthrie, J., Robertson, J.D. and Kornfeld, K. (2012) Lysosome-related organelles in intestinal cells are a zinc storage site in C. elegans. *Cell. Metab.*, **15**, 88–99.
36. Palmiter, R.D., Cole, T.B. and Findley, S.D. (1996) ZnT-2, a mammalian protein that confers resistance to zinc by facilitating vesicular sequestration. *EMBO J.*, **15**, 1784–1791.
37. Falcon-Perez, J.M. and Dell'Angelica, E.C. (2007) Zinc transporter 2 (SLC30A2) can suppress the vesicular zinc defect of adaptor protein 3-depleted fibroblasts by promoting zinc accumulation in lysosomes. *Exp. Cell Res.*, **313**, 1473–1483.
38. Outten, C.E. and O'Halloran, T.V. (2001) Femtomolar sensitivity of metalloregulatory proteins controlling zinc homeostasis. *Science*, **292**, 2488–2492.
39. Lichten, L.A. and Cousins, R.J. (2009) Mammalian zinc transporters: nutritional and physiologic regulation. *Annu. Rev. Nutr.*, **29**, 153–176.

40. McMahon, R.J. and Cousins, R.J. (1998) Regulation of the zinc transporter ZnT-1 by dietary zinc. *Proc. Natl Acad. Sci. USA*, **95**, 4841–4846.
41. Jou, M.Y., Philipps, A.F., Kelleher, S.L. and Lonnerdal, B. (2010) Effects of zinc exposure on zinc transporter expression in human intestinal cells of varying maturity. *J. Pediatr. Gastroenterol. Nutr.*, **50**, 587–595.
42. Palmiter, R.D. and Findley, S.D. (1995) Cloning and functional characterization of a mammalian zinc transporter that confers resistance to zinc. *EMBO J.*, **14**, 639–649.
43. Brown, A.M., Kristal, B.S., Effron, M.S., Shestopalov, A.I., Ullucci, P.A., Sheu, K.F., Blass, J.P. and Cooper, A.J. (2000) Zn2+ inhibits alpha-ketoglutarate-stimulated mitochondrial respiration and the isolated alpha-ketoglutarate dehydrogenase complex. *J. Biol. Chem.*, **275**, 13441–13447.
44. Link, T.A. and von Jagow, G. (1995) Zinc ions inhibit the QP center of bovine heart mitochondrial bc1 complex by blocking a protonatable group. *J. Biol. Chem.*, **270**, 25001–25006.
45. Wudarczyk, J., Debska, G. and Lenartowicz, E. (1999) Zinc as an inducer of the membrane permeability transition in rat liver mitochondria. *Arch. Biochem. Biophys.*, **363**, 1–8.
46. Dineley, K.E., Richards, L.L., Votyakova, T.V. and Reynolds, I.J. (2005) Zinc causes loss of membrane potential and elevates reactive oxygen species in rat brain mitochondria. *Mitochondrion*, **5**, 55–65.
47. Gusdon, A.M., Zhu, J., Van Houten, B. and Chu, C.T. (2012) ATP13A2 regulates mitochondrial bioenergetics through macroautophagy. *Neurobiol. Dis.*, **45**, 962–972.
48. Grunewald, A., Arns, B., Seibler, P., Rakovic, A., Munchau, A., Ramirez, A., Sue, C.M. and Klein, C. (2012) ATP13A2 mutations impair mitochondrial function in fibroblasts from patients with Kufor-Rakeb syndrome. *Neurobiol. Aging*, **33**, 1843 e1841–1847.
49. Schultheis, P.J., Fleming, S.M., Clippinger, A.K., Lewis, J., Tsunemi, T., Giasson, B., Dickson, D.W., Mazzulli, J.R., Bardgett, M.E., Haik, K.L. *et al.* (2013) Atp13a2-deficient mice exhibit neuronal ceroid lipofuscinosis, limited alpha-synuclein accumulation and age-dependent sensorimotor deficits. *Hum. Mol. Genet.*, **22**, 2067–2082.
50. Devine, M.J., Gwinn, K., Singleton, A. and Hardy, J. (2011) Parkinson's disease and alpha-synuclein expression. *Mov. Disord.*, **26**, 2160–2168.
51. Esteves, A.R., Arduino, D.M., Swerdlow, R.H., Oliveira, C.R. and Cardoso, S.M. (2009) Oxidative stress involvement in alpha-synuclein oligomerization in Parkinson's disease cybrids. *Antioxid. Redox Signal.*, **11**, 439–448.
52. Li, W., Jiang, H., Song, N. and Xie, J. (2011) Oxidative stress partially contributes to iron-induced alpha-synuclein aggregation in SK-N-SH cells. *Neurotox. Res.*, **19**, 435–442.
53. Freeman, D., Cedillos, R., Choyke, S., Lukic, Z., McGuire, K., Marvin, S., Burrage, A.M., Sudholt, S., Rana, A., O'Connor, C. *et al.* (2013) Alpha-synuclein induces lysosomal rupture and cathepsin dependent reactive oxygen species following endocytosis. *PLoS ONE*, **8**, e62143.
54. Schissel, S.L., Keesler, G.A., Schuchman, E.H., Williams, K.J. and Tabas, I. (1998) The cellular trafficking and zinc dependence of secretory and lysosomal sphingomyelinase, two products of the acid sphingomyelinase gene. *J. Biol. Chem.*, **273**, 18250–18259.
55. Macauley, S.L., Sidman, R.L., Schuchman, E.H., Taksir, T. and Stewart, G.R. (2008) Neuropathology of the acid sphingomyelinase knockout mouse model of Niemann-Pick A disease including structure-function studies associated with cerebellar Purkinje cell degeneration. *Exp. Neurol.*, **214**, 181–192.
56. Jeong, H., Then, F., Melia, T.J. Jr, Mazzulli, J.R., Cui, L., Savas, J.N., Voisine, C., Paganetti, P., Tanese, N., Hart, A.C. *et al.* (2009) Acetylation targets mutant huntingtin to autophagosomes for degradation. *Cell*, **137**, 60–72.
57. Tsunemi, T., Ashe, T.D., Morrison, B.E., Soriano, K.R., Au, J., Roque, R.A., Lazarowski, E.R., Damian, V.A., Masliah, E. and La Spada, A.R. (2012) PGC-1alpha rescues Huntington's disease proteotoxicity by preventing oxidative stress and promoting TFEB function. *Sci. Transl. Med.*, **4**, 142ra197.